# Reachable Power Flow: Theory to Practice

Yifan Zhou D, Member, IEEE, and Peng Zhang D, Senior Member, IEEE

Abstract—Reachable power flow (ReachFlow) is a newly developed formal method for enclosing the complete set of uncertain power flow states. To enable ReachFlow's transition from theory to practice, the paper makes three major contributions: (1) both small- and large- signal stability proofs for the ordinary differential equation (ODE)-based power flow are devised to theoretically ensure the robustness of ReachFlow; (2) a model-order-reduction-empowered ReachFlow(ReachFlow<sup>R</sup>) algorithm is created for analyzing interested regions in large power systems; and (3) a parallel ReachFlow (ReachFlow<sup>P</sup>) algorithm is established to scale up ReachFlow for the accurate analysis of very large power systems. Extensive case studies are performed on a series of test systems, ranging from a 33-bus microgrid to a 2,000-bus power system, to thoroughly verify the correctness, efficacy and practicality of ReachFlow in formally verifying microgrid and macrogrid power flows as well as power flow control strategies.

Index Terms—Reachable power flow, reachability, uncertainty, reduced-order ReachFlow, parallel ReachFlow.

#### I. INTRODUCTION

ODERN power system is evolving with ever-increasing penetration of renewable energy (RE) sources [1]. Recently, Europe, the USA and China have envisioned respectively their 100% [2], 80% [3] and 60% [4] RE-supported power grids by 2050. Dependable power flow analysis under unprecedented uncertainties has thus been a fundamental need for the design, planning and operations of power systems.

There exist two main types of approaches to analyzing power flows under uncertainties. Monte Carlo simulations [5]–[8] suffer from prohibitively high computational burden for high-dimensional uncertainties [9] and from overly optimistic assessments because they are unable to sample the infinitely many scenarios. Analytical approaches such as certain probabilistic power flow tools calculate discrete distributions of power flows [10], [11]. However, mainly due to the inability to capture tail events, the probabilistic analysis results can not include all the possible power flow solutions, which therefore fail to provide conservative assessment. Alternatively, set-based static power flow methods formulate uncertainties using intervals [12], [13], ellipsoids [14], [15] or zonotopes [16], [17], yet their

Manuscript received May 24, 2020; revised September 7, 2020; accepted October 11, 2020. Date of publication October 14, 2020; date of current version April 19, 2021. This work was supported by the National Science Foundation under Grants ECCS-1831811 and OIA-2040599. Paper no. TPWRS-00852-2020. (Corresponding author: Peng Zhang.)

The authors are with the Department of Electrical and Computer Engineering, Stony Brook University, Stony Brook, NY 11794 USA (e-mail: yifan.zhou.1@stonybrook.edu; p.zhang@stonybrook.edu).

Color versions of one or more of the figures in this article are available online at https://ieeexplore.ieee.org.

Digital Object Identifier 10.1109/TPWRS.2020.3031196

convergence issues inherited from iterative nonlinear solvers and the non-conservativeness risks prohibit their adoption in power system operations.

Recently, a novel *reachable power flow* (*ReachFlow*) theory has been emerging [18] to rigorously enclose the uncertain power flow states via a single reachability calculation, rendering repetitious Monte Carlo sampling unnecessary. Although the proof-of-concept of *ReachFlow* on a small microgrid is successful [18], its applicability to real power systems is a major difficulty due to the computational expense of high-dimensional reachability analysis [19]. Further, the robustness of *ReachFlow* is yet to be formally proved. To tackle the barriers to practical use of *ReachFlow* for large systems, this paper thoroughly enhances *ReachFlow* in three aspects:

- The stability of the ordinary differential equation -based power flow (ODE-PF) model is formally proved.
  - The key innovation of *ReachFlow* is obtaining reachable power flow results by performing reachability analysis on the virtual dynamics of ODE-PF. The proofs of small-and large-signal stability of the ODE-PF dynamics offer strong theoretical guarantees for successful applications of *ReachFlow* to arbitrary power flow cases.
- A reduced-order ReachFlow(ReachFlow<sup>R</sup>) is devised to allow for ultra-efficient reachability analysis on the reduced-order ODE-PF dynamics.
  - By projecting the high-dimensional reachable set evolution to a subspace expanded by the vital power flow states,  $ReachFlow^R$  enables large-scale ReachFlow analysis.
- A parallel ReachFlow(ReachFlow<sup>P</sup>) algorithm is further established to empower scalable and accurate reachability analysis with the parallel computing architecture.

The original high-dimensional *ReachFlow* for solving very large scale power flow problem is decomposed to a set of sub-*ReachFlow* tasks suitable for concurrent processing.

The remainder of this paper is organized as follows. Section II introduces ODE-PF and theoretically proves its stability. Section III recapitulates the basic ReachFlow, while Section IV and V respectively devise  $ReachFlow^R$  and  $ReachFlow^P$ . Finally, case studies are discussed in Section VI.

#### II. ODE-BASED POWER FLOW MODEL

A provably stable ODE-PF model is devised to quantify the propagation of uncertainties in the power flow solution.

- A. Power Flow Formulation With Frequency/Voltage Control
- 1) Macrogrid Power Flow Model: We extend the traditional power flow formulation for bulk power system by adding the

 $0885\text{-}8950 \circledcirc 2020 \text{ IEEE. Personal use is permitted, but republication/redistribution requires \text{ IEEE permission.}} \\ \text{See https://www.ieee.org/publications/rights/index.html for more information.}$ 

primary frequency control for specific generators, as follows:

$$P_i = P_i^* + k_i(f^* - f) + u_i \tag{1}$$

where  $P_i$  denotes the active power generation of generator i; f is the system frequency;  $P_i^*$  and  $f^*$  respectively denote the nominal values of  $P_i$  and f;  $k_i$  is the frequency regulation coefficient;  $u_i$  formulates the uncertainty input due to the RE resources. For the fully-controllable generators,  $u_i = 0$ .

2) Microgrid Power Flow Model: A complete microgrid power flow is an augmentation of traditional power flow model with hierarchical control models [20]. The hierarchical control for active power-frequency regulation of distributed energy resource (DER) is formulated as:

$$\omega_i = \omega_i^* - m_{p,i} (P_i - (P_i^* + u_i)) + \Omega_i$$
 (2a)

$$\omega_i - \omega_i^* + \sum_{j \in S^{DER}} a_{ij} (\Omega_i - \Omega_j) = 0$$
 (2b)

where  $\omega_i$  denotes the angular frequency of DER i;  $\Omega_i$  is the secondary control signal of DER i which can be achieved by distributed consensus [20];  $\omega_i^*$  and  $P_i^*$  respectively denote the nominal angular frequency and active power;  $u_i$  represents the RE uncertainty;  $m_{p,i}$  is the droop gain;  $\mathcal{S}^{DER}$  denotes the set of DERs;  $a_{ij}$  denotes the active power sharing coefficient between DER i and DER j.

Further, the reactive power-voltage control is expressed as:

$$E_i = E_i^* - n_{q,i}Q_i + e_i \tag{3a}$$

$$\beta_i(E_i - E_i^*) + \sum_{j \in S^{DER}} b_{ij}(Q_i/Q_i^* - Q_j/Q_j^*) = 0$$
 (3b)

where  $E_i$  is the output voltage of DER i;  $e_i$  is the secondary control signal;  $E_i^*$  and  $Q_i^*$  respectively denote the nominal voltage amplitude and reactive power output;  $n_{q,i}$  is the droop gain;  $\beta_i$  and  $b_{ij}$  are the reactive power sharing coefficients.

A complete steady-state model for DER controls with power, current and voltage controls can be found in [21].

## B. ODE-Based Power Flow (ODE-PF) Formulation

The power flow models above can be abstracted into:

$$\boldsymbol{h}(\boldsymbol{x}, \boldsymbol{u}) = 0 \tag{4}$$

where x denotes state variables, e.g., power generation, voltage, current, system frequency; u denotes the uncertainties.

The Newton-Raphson (NR) iteration can then be derived as:

$$x_{k+1} = x_k - (J_h(x_k, u))^{-1}h(x_k, u)$$
 (5)

where  $x_k$  denotes the value of x at the  $k^{th}$  iteration;  $J_h = \partial h/\partial x|_{x=x_k}$  denotes the Jacobian matrix of h at point  $x_k$ .

The discrete dynamics in (5) can be viewed as an abstraction of a continuous dynamics as follows:

$$\dot{\boldsymbol{x}}(t) = -(\boldsymbol{J}_h(\boldsymbol{x}(t), \boldsymbol{u}))^{-1} \boldsymbol{h}(\boldsymbol{x}(t), \boldsymbol{u}) =: \boldsymbol{f}_x(\boldsymbol{x}(t), \boldsymbol{u}) \quad (6)$$

where t refers to time by viewing the number of iterations as continuous.

The virtual dynamics in (6) is a mathematical equivalent to the NR iterations rather than an actual dynamic process, which is called an ODE-based power flow (ODE-PF) model. It inherently reflects the propagation of uncertainties.

#### C. Stability Proof of the ODE-PF Dynamics

Because ODE-PF is a basis of *ReachFlow* (see Section III), stable ODE-PF dynamics can ensure the convergence of numerical integral in *ReachFlow*. To this end, the small- and large-signal stability of ODE-PF is proved as follows.

1) Small-Signal Stability: An arbitrary  $\hat{u}$  and the corresponding power flow solution  $\hat{x}$  contribute to an equilibrium point of the ODE-PF model, i.e.  $f_x(\hat{x},\hat{u}) = 0$ . Eigenvalues of the state matrix at  $\hat{x}$  can be used to verify the small-signal stability.

Based on (6), we have  $J_h f_x = -h$ . Taking partial derivative with respect to x yields the following:

$$J_{h} \frac{\partial f_{x}}{\partial x} + \frac{\partial J_{h}}{\partial x} f_{x} = -\frac{\partial h}{\partial x} \Longrightarrow$$

$$\frac{\partial f_{x}}{\partial x}|_{(\hat{x},\hat{u})} = -J_{h}^{-1} \left( \frac{\partial h}{\partial x} + \frac{\partial J_{h}}{\partial x} f_{x} \right) = -J_{h}^{-1} J_{h} = -I$$
(7)

Hence, all the eigenvalues of ODE-PF at any equilibrium point definitely have negative real parts, which verifies the asymptotically stability of ODE-PF in small neighbourhoods.

2) Large-Signal Stability: The large-signal stability of the ODE-PF dynamics is proved as: a) ODE-PF is Lyapunov stable at any  $\hat{x}$ ; b) ODE-PF is asymptotically stable at  $\hat{x}$ , if  $\hat{u}$  leads to a unique power flow solution  $\hat{x}$ .

Define the difference between the current states and the equilibrium point  $\hat{x}$  as  $\Delta x = x - \hat{x}$ . The dynamics of  $\Delta x$  can be readily constructed:

$$\frac{\mathrm{d}\Delta x}{\mathrm{dt}} = -(\boldsymbol{J}_h(\Delta x + \hat{\boldsymbol{x}}, \boldsymbol{u}))^{-1} \boldsymbol{h}(\Delta x)$$
(8)

where  $h(\Delta x) = h(\Delta x + \hat{x}, u)$ .

Considering the following Lyapunov function:

$$V(\Delta \mathbf{x}) = \frac{1}{2} \mathbf{h} (\Delta \mathbf{x})^T \mathbf{h} (\Delta \mathbf{x}) + \epsilon$$
 (9)

where  $\epsilon$  is a small positive constant ensuring  $V(\Delta x)$  to be positive definite. The time derivative of V(x) is computed as:

$$\dot{V} = \frac{\partial V}{\partial \Delta x} \frac{d\Delta x}{dt} = \frac{\partial V}{\partial h} \frac{\partial h}{\partial \Delta x} \frac{d\Delta x}{dt} = \frac{\partial V}{\partial h} \frac{\partial h}{\partial x} \frac{d\Delta x}{dt} 
= h(\Delta x)^T J_h(-J_h^{-1} h(\Delta x))$$

$$= -h(\Delta x)^T h(\Delta x) < 0$$
(10)

Hence,  $\dot{V}$  is negative semi-definite, which proves the Lyapunov stability of ODE-PF dynamics around an arbitrary equilibrium point  $\hat{x}$ .

Further, if  $\hat{u}$  leads to a unique power flow solution  $\hat{x}$ , we have  $h(x, \hat{u}) \neq 0$  if  $x \neq \hat{x}$ , which yields the following:

$$\dot{V} < 0, \ \forall x \in \mathcal{X} \setminus \{\hat{x}\}\$$
 (11)

where  $\mathcal{X}$  is the domain of x. Hence,  $\hat{x}$  is asymptotically stable in  $\mathcal{X}$ . This indicates that the crisp power flow solution without uncertainty is in the stability region of  $\hat{x}$ . Consequently, the

ODE-PF integrating from the crisp power flow solution (see (14)) definitely converges to  $\hat{x}$  for an arbitrary uncertainty  $\hat{u}$ .

The two proofs theoretically guarantee that *ReachFlow* is a non-divergent power flow under small and large uncertainties.

#### III. REACHABLE POWER FLOW

This section recapitulate the *ReachFlow* methodology [18] which was devised by the authors to establish a provably enclosure of all the uncertain power flow solutions.

#### A. ReachFlow Formulation

Incorporating the DER uncertainties  $\boldsymbol{u}$  in the ODE-PF model formulates the augmented ODE-PF model:

$$\begin{cases} \dot{\boldsymbol{x}}(t) = -(\boldsymbol{J}_h(\boldsymbol{x}(t), \boldsymbol{u}(t)))^{-1} \boldsymbol{h}(\boldsymbol{x}(t), \boldsymbol{u}(t)) & (12a) \\ \dot{\boldsymbol{u}}(t) = \boldsymbol{0} & (12b) \end{cases}$$

Equation (12b) means that the uncertainty input u remains constant during a single run of power flow. The rationale behind (12b) is that during the NR iteration, the uncertainty input should not be changed because (12a) corresponds to the solution process of a single power flow under a specific uncertain scenario.

Functionally, (12) is abstracted as:

$$\dot{\boldsymbol{z}}(t) = \boldsymbol{f}(\boldsymbol{z}(t)) \tag{13}$$

Here, z = [x; u] denotes the augmented power flow states;  $f(z) = [f_x(x, u); f_u(x, u)]$  formulates the augmented ODE-PF dynamics;  $f_u = 0$ .

With arbitrary u, the steady state of (13) exactly refers to the power flow solution with a specific u. Hence, finding the set of all possible power flows is equivalent to finding the possible steady states of the dynamics in (13).

The recognition above leads to the reachable power flow (*ReachFlow*) set defined as:

$$\mathcal{R}_{PF} = \left\{ \boldsymbol{z} = \int_0^\infty \boldsymbol{f}(\boldsymbol{z}(t)) dt \mid \boldsymbol{x}(0) \in \mathcal{X}^0, \boldsymbol{u} \in \mathcal{U}^0 \right\} \quad (14)$$

where z and f(z) are defined in (13);  $\mathcal{X}^0$  and  $\mathcal{U}^0$  are the set of the initial states and uncertainty inputs.  $\mathcal{R}_{PF}$  exactly characterizes the set of all possible power flows regarding the uncertain input  $\mathcal{U}^0$ .

## B. ReachFlow Algorithm

Through the definition of  $\mathcal{R}_{PF}$ , the reachable set [22] of continuous time t is defined as:

$$\mathcal{R}(t) = \left\{ \boldsymbol{z}(t) = \int_0^t f(\boldsymbol{z}(\tau)) d\tau \mid \boldsymbol{z}(0) \in \mathcal{Z}^0 \right\}$$
 (15)

where  $\mathcal{Z}^0 = \mathcal{X}^0 \otimes \mathcal{U}^0$ ;  $\otimes$  denotes the Cartesian product. In this paper, the uncertainty inputs are governed by an unknown-but-bounded set  $\mathcal{U}^0$ , and zonotope is adopted for set modeling for its efficiency in linear transformation and Minkowski addition [23].

The nonlinear dynamics in (13) can be over-approximated by the first-order Taylor term and the Lagrange remainder:

$$\dot{z} \in \underbrace{f(z^*) + A(z - z^*)}_{\text{linear abstraction}} + \underbrace{\mathcal{L}(z - z^*)}_{\text{linearization remainder}}$$
(16)

# **Algorithm 1:** ReachFlow Algorithm.

```
Initialization: \mathcal{X}^0 = \{x_0\} by solving Eq. (4) without uncertainty, \mathcal{U}^0, \tau, k = 0;

while l do

| k = k + 1;
| Update <math>\mathcal{R}_k by Eq. (17);

if isequal(\mathcal{R}_k, \mathcal{R}_{k-1}) then
| \mathcal{R}_{PF} = \mathcal{R}_k;
| break;
| end
9 end
10 Output: \mathcal{R}_{PF};
```

where  $z^*$  is the linearization point;  $A = \partial f/\partial z|_{z=z^*}$  is the Jacobian matrix;  $\mathcal{L}$  is the linearization error due to the Lagrange remainder.

Hence, the reachable set during time interval  $[k\tau, (k+1)\tau]$   $(k \in \mathbb{N})$  can be over-approximated by:

$$\mathcal{R}([k\tau, (k+1)\tau]) \triangleq \mathcal{R}_k \subseteq \mathcal{R}_k^{lin} \oplus \mathcal{R}_k^{err}$$
 (17)

where  $\oplus$  denotes the Minkowski addition between two sets.  $\mathcal{R}_k^{lin}$  and  $\mathcal{R}_k^{err}$  respectively denote the over-approximated reachable sets of the linear abstraction and the linearization error, which are computed by function 'LinearReach' and function 'ErrorReach' as detailed in Appendix VII.

The reachability analysis leads to **Algorithm 1**. ReachFlow is initialized by the conventional power flow calculation without uncertainty. Then, the reachable set of the ODE-PF model is calculated step by step, which reflects the propagation of the uncertainty set  $\mathcal{U}^0$  during power flow calculation. The ReachFlow algorithm converges when the reachable set becomes stable. The reachable set at the last time step will be the final ReachFlow which is the rigorous enclosure of all possible power flow solutions under  $\mathcal{U}^0$ .

# IV. REDUCED-ORDER REACHABLE POWER FLOW

Even though ReachFlow is more efficient than other uncertain power flow approaches, its utility application is hindered by the high computational cost in calculating large power systems. In practice, utility or ISO engineers usually only need a few pivotal power flow states in regions of interest for operations and planning purposes. Motivated by this observation, a reduced-order ReachFlow ( $ReachFlow^R$ ) algorithm is devised. Rather than involving all the power flow variables,  $ReachFlow^R$  performs the reachability analysis in the subspace spanned by a reduced number of power flow features.

# A. Order Reduction of ReachFlow Formulation

Denote  $x_r$  as the reduced-order power flow states selected for ReachFlow analysis. Denote  $z_r = [x_r; u]$  as the augmented reduced-order power flow states. Define the projection matrix  $\Psi_r$  satisfying  $z_r = \Psi_r z$ , which maps the reduced-order states  $z_r$  to the complete states  $z_r$ .  $ReachFlow^R$  is then defined as:

$$\mathcal{R}_{PF,r} = \left\{ \boldsymbol{z}_r = \int_0^\infty \Psi_r \boldsymbol{f}(\boldsymbol{z}(t)) dt \mid \boldsymbol{z}(0) \in \mathcal{Z}^0 \right\}$$
 (18)

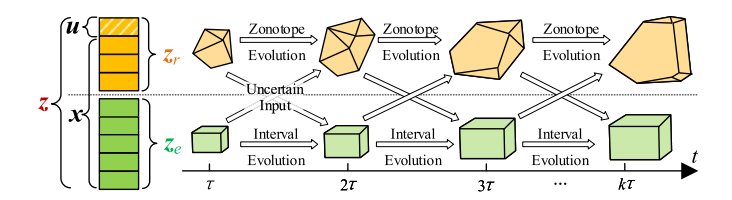


Fig. 1. Schematic diagram of reduced-order ReachFlow.

Denote  $z_e$  as the eliminated states in z and define the projection matrix  $\Psi_e$  satisfying  $z_e = \Psi_e z$ . It can be readily proved that  $z = \Psi_r^T z_r + \Psi_e^T z_e$ .

 $ReachFlow^R$  is illustrated in Fig. 1. By dividing the overall augmented power flow states z into  $z_r$  and  $z_e$ ,  $ReachFlow^R$  only computes the reachable set of  $z_r$ , i.e.,  $\mathcal{R}_{PF,r}$  illustrated by the yellow zonotopes. However, the dynamics of  $z_r$  inherently involves  $z_e$ . Hence, the bounds of  $z_e$  is also estimated, as depicted by the green intervals, and serves as an uncertainty input for the reachability analysis of  $z_r$ . By analogy with (16), the linearization of ODE-PF model is perform on the reduced-order power flow states:

$$\dot{z}_r \in \underbrace{f_r(z^*) + A_{rr}(z_r - z_r^*)}_{\text{linear abstraction}} + \underbrace{A_{re}(z_e - z_e^*) + \Psi_r \mathcal{L}}_{\text{order reduction remainder}}$$
(19)

where 
$$\boldsymbol{f}_r(\boldsymbol{z}^*) = \Psi_r \boldsymbol{f}(\boldsymbol{z}^*)$$
;  $\boldsymbol{A}_{rr} = \Psi_r \boldsymbol{A} \Psi_r^T$ ;  $\boldsymbol{A}_{re} = \Psi_r \boldsymbol{A} \Psi_e^T$ .

Equation (19) indicates that the over-approximated dynamics of  $z_T$  also consists of a linearized part as well as a remainder part, with exactly the same form as (16). Hence, the reachable set algorithm in Section III also applies:

$$\mathcal{R}_r([k\tau, (k+1)\tau]) \triangleq \mathcal{R}_{k,r} \subseteq \mathcal{R}_{k,r}^{lin} \oplus \mathcal{R}_{k,r}^{err}$$
 (20)

Here  $\mathcal{R}_{k,r}^{lin}$  is the reachable set of the linear abstraction in (19) and  $\mathcal{R}_{k,r}^{lin}$  = LinearReach( $\mathcal{R}_r(k\tau), \boldsymbol{z}_r^*, \boldsymbol{f}_r, \boldsymbol{A}_{rr}, \tau$ ) (see (33)). Since the zonotope evolution is performed in a reduced-order space, the computing efficiency is significantly enhanced.

Set  $\mathcal{R}_{k,r}^{err}$  refers to the reachable set of the remainder term in (19) comprising both the Lagrange remainder (i.e.,  $\Psi_r \mathcal{L}(z-z^*)$ ) and the impact of the eliminated power flow states (i.e.,  $A_{re}(z_e-z_e^*)$ ). Letting  $\mathcal{L}_{r1}=A_{re}(z_e-z_e^*)$  and  $\mathcal{L}_{r2}=\Psi_r \mathcal{L}$ , one can yield the following over-approximation:

$$|\mathcal{L}_{r1}| \le |\mathbf{A}_{re}| \sup(\mathbf{z}_e - \mathbf{z}_e^*) \triangleq \overline{\mathcal{L}}_{r1}, \mathcal{L}_{r2} \le \Psi_r \overline{\mathcal{L}} \triangleq \overline{\mathcal{L}}_{r2}$$
 (21)

where sup denotes the supremum operator. Hence,  $\mathcal{R}_{k,r}^{err} = \operatorname{ErrorReach}(\overline{\mathcal{L}}_{r1}, A_{rr}, \tau) \oplus \operatorname{ErrorReach}(\overline{\mathcal{L}}_{r2}, A_{rr}, \tau)$ .

# B. Reduced-Order ReachFlow Algorithm

Algorithm 2 summarizes the  $ReachFlow^R$  algorithm.  $ReachFlow^R$  performs the same initialization as ReachFlow, to establish the set of initial power flow states  $\mathcal{X}^0$  and uncertainty inputs  $\mathcal{U}^0$  by algebraic calculation. Then the reduced-order power flow states  $\boldsymbol{x}_r$  is selected by the power engineer for specific reachability analysis, and the corresponding projection matrices are prepared. Next, the reduced-order reachable set in (18) is calculated step by step until convergence to quantify the impact of  $\mathcal{U}^0$  on  $\boldsymbol{x}_r$ .

# **Algorithm 2:** ReachFlow<sup>R</sup> Aalgorithm.

```
Initialization: \mathcal{X}^0 = \{x_0\}, \, \mathcal{U}^0, \, \tau, \, k = 0 \; ;
2 Select the reduced-order power flow states \boldsymbol{x}_r;
3 Prepare projection matrices \Psi_r, \, \Psi_e;
4 while I do
5 k = k + 1;
6 Calculate \boldsymbol{f}_r, \, \boldsymbol{A}_{rr} by Eq. (19) and \overline{\mathcal{L}}_{r1}, \, \overline{\mathcal{L}}_{r2} by (21);
7 Update \mathcal{R}_{k,r} by Eq. (20);
8 if isequal(\mathcal{R}_{k,r}, \mathcal{R}_{k-1,r}) then
9 \mathcal{R}_{PF,r} = \mathcal{R}_{k,r};
10 break;
11 end
12 end
13 Output : \mathcal{R}_{PF,r};
```

#### V. PARALLEL REACHABLE POWER FLOW

Another potent approach to accelerating *ReachFlow* is to exploit the parallel computing capability of the ubiquitous multi-core processors. This section devises a parallel *Reach-Flow* (*ReachFlow*<sup>P</sup>) to over-approximate the high-dimensional reachable set by the Cartesian product of a set of lower-dimensional reachable sets. Therefore, the serial computation of *ReachFlow* is broken into 'independent' sub-*ReachFlow* s with the dependencies serving as the uncertainty inputs that can be processed concurrently.

#### A. Partition of ReachFlow Formulation

Suppose that the power flow vector x is partitioned into P disjoint subsets, i.e.,  $x_1, x_2, \ldots, x_P$ . This subsection devises a  $ReachFlow^P$  formulation, which decomposes the ReachFlow set in Section III into discrete sub-sets for each  $x_p$ .

For arbitrary  $x_p$ , define  $z_p = [x_p; u]$  as the  $p^{th}$  subset of augmented power flow states. Define the projection matrix  $\Psi_p$  satisfying  $z_p = \Psi_p z$ , which maps the  $p^{th}$  subset of augmented power flow states to the complete augmented power flow states. From (13), the ODE-PF for  $z_p$  can be formulated as:

$$\dot{\boldsymbol{z}}_{p} = \Psi_{p} \boldsymbol{f}(\boldsymbol{z}), \ \forall p \tag{22}$$

Correspondingly, the *ReachFlow* set for  $z_p$ , i.e., the  $p^{th}$  sub-*ReachFlow*, is formulated as:

$$\mathcal{R}_{PF,p} = \left\{ \boldsymbol{z}_p = \int_0^\infty \Psi_p \boldsymbol{f}(\boldsymbol{z}(t)) dt \mid \boldsymbol{z}(0) \in \mathcal{Z}^0 \right\}, \ \forall p \ (23)$$

Define projection matrices  $\psi_p$  satisfying  $\mathbf{z}_p = \psi_p[\mathbf{x}; \mathbf{0}]$ , and  $\psi_u$  satisfying  $\mathbf{u} = \psi_u \mathbf{z}$ . It can be readily proved that  $\mathbf{z} = \sum_{p=1}^P \psi_p^T \mathbf{z}_p + \psi_u^T \mathbf{u}$ . Hence, based on each sub-*ReachFlow*, the complete *ReachFlow* can be conservatively reconstructed as:

$$\mathcal{R}_{PF} = \sum\nolimits_{p=1}^{P} \psi_{p}^{T} \mathcal{R}_{PF,p} \oplus \psi_{u}^{T} \mathcal{U}^{0}$$
 (24)

 $ReachFlow^P$  is illustrated in Fig. 2. By dividing the overall power flow states into P subsets,  $ReachFlow^P$  computes the reachable sets of each  $z_p$  in parallel on different cores, i.e.,  $\mathcal{R}_{PF,p}$  as illustrated by the zonotopes of different colors. The dependency between each subset of power flow states is modelled as the uncertainty inputs. After obtaining each sub-ReachFlow,

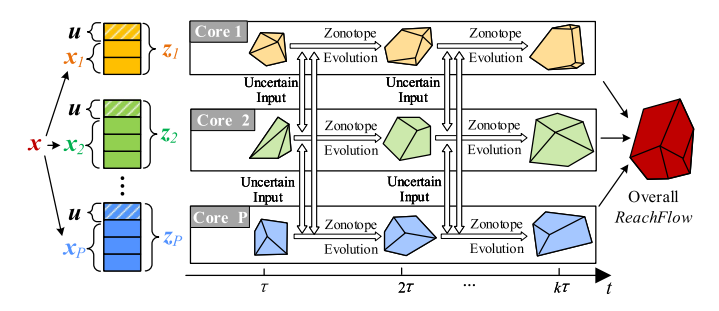


Fig. 2. Schematic diagram of parallel ReachFlow.

the overall *ReachFlow* will be constructed by the Cartesian product of the reachable set on each  $z_p$ .

To compute each sub-*ReachFlow*, the ODE-PF of  $z_p$  is linearized by analogy with (16):

$$\dot{\boldsymbol{z}}_{p} \in \Psi_{p}(\boldsymbol{f}(\boldsymbol{z}^{*}) + \boldsymbol{A}(\boldsymbol{z} - \boldsymbol{z}^{*}) + \mathcal{L}(\boldsymbol{z} - \boldsymbol{z}^{*})) 
= \Psi_{p}\boldsymbol{f}(\boldsymbol{z}^{*}) + \Psi_{p}\boldsymbol{A}\Psi_{p}^{T}(\boldsymbol{z}_{p} - \boldsymbol{z}_{p}^{*}) 
+ \Psi_{p}\boldsymbol{A}\sum_{j\neq p}\psi_{j}^{T}(\boldsymbol{z}_{j} - \boldsymbol{z}_{j}^{*}) + \Psi_{p}\mathcal{L}(\boldsymbol{z} - \boldsymbol{z}^{*})$$

$$= \underbrace{\boldsymbol{f}_{p} + \boldsymbol{A}_{p}(\boldsymbol{z}_{p} - \boldsymbol{z}_{p}^{*})}_{\text{linear abstraction}} + \underbrace{\mathcal{L}_{p}(\boldsymbol{z} - \boldsymbol{z}^{*})}_{\text{parallel remainder}} \tag{25}$$

Here, the relationship  $\boldsymbol{z} = \boldsymbol{\Psi}_p^T \boldsymbol{z}_p + \sum_{j \neq p} \boldsymbol{\psi}_j^T \boldsymbol{z}_j$  is applied in above derivation;  $\boldsymbol{z}^*$ ,  $\boldsymbol{A}$  and  $\boldsymbol{\mathcal{L}}$  are respectively the linearization point, Jacobian matrix and Lagrange reminder as defined in (16);  $\boldsymbol{f}_p = \boldsymbol{\Psi}_p \boldsymbol{f}(\boldsymbol{z}^*)$ ,  $\boldsymbol{A}_p = \boldsymbol{\Psi}_p \boldsymbol{A} \boldsymbol{\Psi}_p^T$  and  $\boldsymbol{\mathcal{L}}_p = \boldsymbol{\Psi}_p \boldsymbol{A} \sum_{j \neq p} \boldsymbol{\psi}_p^T (\boldsymbol{z}_j - \boldsymbol{z}_j^*) + \boldsymbol{\Psi}_p \mathcal{L}(\boldsymbol{z} - \boldsymbol{z}^*)$ .

Equation (25) is in the identical form with (16). Hence, the reachability analysis in Section III-A can be readily performed. More specifically, the reachset for  $z_p$  during time interval  $[k\tau, (k+1)\tau]$  is formulated by:

$$\mathcal{R}_p([k\tau, (k+1)\tau]) \triangleq \mathcal{R}_{k,p} \subseteq \mathcal{R}_{k,p}^{lin} \oplus \mathcal{R}_{k,p}^{err}, \ \forall p$$
 (26)

Set  $\mathcal{R}^{lin}_{k,p}$  refers to the reachable set of the linear abstraction in (25). According to (33),  $\mathcal{R}^{lin}_{k,p}$  is computed as:

$$\mathcal{R}_{k,p}^{lin} = \text{LinearReach}(\mathcal{R}_p(k\tau), \boldsymbol{z}_p^*, \boldsymbol{f}_p, \boldsymbol{A}_p, \tau)$$
 (27)

Obviously, (27) is independent for each  $z_p$  and hence parallelenabled. Further, the reachable set evolution of (33) occupies the most computational resources due to the complicated zonotope calculation. Hence, the parallelization from (33) to (27) will substantially enhance the *ReachFlow* efficiency.

Set  $\mathcal{R}_{k,p}^{err}$  refers to the reachable set of the remainder term, which includes both the Lagrange remainder  $\mathcal{L}_{p1}$  and the parallel computing remainder  $\mathcal{L}_{p2}$  (i.e., the impact of  $z_j$  on  $z_p$ ). The following over-approximation applies for  $\mathcal{L}_p$ :

$$|\mathcal{L}_{p1}| \leq \Psi_p |\mathcal{L}| \triangleq \overline{\mathcal{L}}_{p1}$$

$$|\mathcal{L}_{p2}| \leq \Psi_p |\mathbf{A}| \sum_{j \neq p} \psi_p^T \sup(\mathbf{z}_j - \mathbf{z}_j^*) \triangleq \overline{\mathcal{L}}_{p2}$$
(28)

Note that  $\overline{\mathcal{L}}_{p1}$  and  $\overline{\mathcal{L}}_{p2}$  involve all the power flow states (i.e.,  $z_j$ ) as well as the overall Lagrange remainder; so it

```
Algorithm 3: ReachFlow<sup>P</sup> Algorithm.
```

```
Initialization: \mathcal{X}^0 = \{x_0\}, \, \mathcal{U}^0, \, \tau, \, k = 0, \, flag_p = 0 (\forall p);
    Partition power flow states to x_1, x_2, \ldots, x_P;
    Prepare projection matrices \Psi_p(\forall p), \psi_p(\forall p), \psi_u;
    while (\neg flag_1)||(\neg flag_2)||\dots||(\neg flag_P) do
            > Coordination Tasks:
            Calculate \underline{f}(z^*), A = \partial f/\partial z |_{z=z^*} by Eq. (16) ;
            Calculate \overline{\mathcal{L}}_{p1}, \overline{\mathcal{L}}_{p2} (\forall p) by Eq. (28);
            > Parallel Tasks:
10
11
            parfor p=1:P
                   Update \mathcal{R}_{k,p} by Eq. (26);
12
                    \begin{array}{l} \text{if } \textit{isequal}(\mathcal{R}_{k,p},\mathcal{R}_{k-1,p}) \text{ then} \\ \mid \mathcal{R}_{PF,p} = \mathcal{R}_{k,p}, \textit{flag}_p = 1 \ ; \end{array} 
14
15
16
                    \int flag_p = 0 ;
17
18
19
20
    end
    Output : \mathcal{R}_{PF} by Eq.(24);
```

can not be parallelized. Fortunately, (28) performs the interval calculation, which is far more effortless compared with the zonotope calculation. Hence,  $\mathcal{R}_{k,p}^{err}$  is enclosed by  $\mathcal{R}_{k,p}^{err} = \operatorname{ErrorReach}(\overline{\mathcal{L}}_{p1}, \boldsymbol{A}_{p}, \tau) \oplus \operatorname{ErrorReach}(\overline{\mathcal{L}}_{p2}, \boldsymbol{A}_{p}, \tau)$ .

# B. Parallel ReachFlow Algorithm

Algorithm 3 presents the  $ReachFlow^P$  algorithm. Different from ReachFlow or  $ReachFlow^R$ , the reachability analysis in  $ReachFlow^P$  is divided into a coordination module and parallel tasks. The coordination calculation prepares the overall Jacobian matrix and Lagrange remainder around the linearization point. Then, the parallel calculation updates the reachable set of each  $\boldsymbol{z}_p$  independently with the linearization information released by the centralized calculation. The algorithm terminates until each sub-ReachFlow converges.

## VI. CASE STUDY

ReachFlow, ReachFlow<sup>R</sup> and ReachFlow<sup>P</sup> are developed in MATLAB R2019b on the basis of CORA [24] and run on a 3.70 GHz PC with 32 GB RAM and 8 cores. ReachFlow<sup>P</sup> is implemented via the MATLAB Parallel Computing Toolbox.

# A. Validity of ReachFlow Methodology

*ReachFlow* is verified on multiple microgrid and macrogrids to exhibit its validity, efficacy and universality.

1) Microgrid ReachFlow: ReachFlow is first validated on a 33-bus microgrid [25] including 5 droop-controlled DERs. A 20% of uncertainty is set for each DER by default.

Fig. 3 illustrates the calculation process of *ReachFlow*. Starting from the crisp power flow solution  $x_0$  without uncertainty, the reachable set successively expands as uncertainty impact propagates in the ODE-PF dynamics. The final *ReachFlow* is obtained once the zonotope stabilizes at the  $8^{th}$  step. Fig. 4 shows

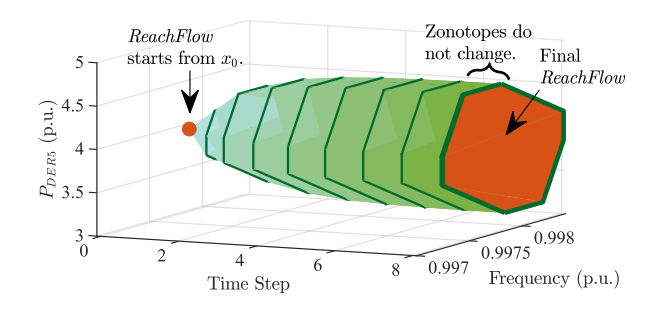


Fig. 3. Reachable set evolution during the 'iteration dynamic' ( $P_{DER5}$ : active power output of DER5).

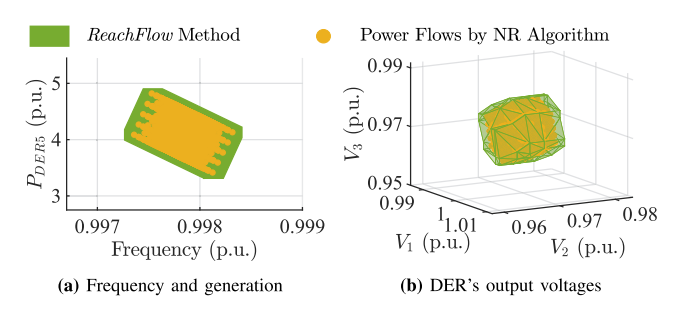


Fig. 4. ReachFlow result in the modified 33-bus microgrid ( $P_{DERi}$ : active power output of the  $i_{th}$  DER;  $V_i$ : output-voltage magnitudes of the  $i_{th}$  DER).

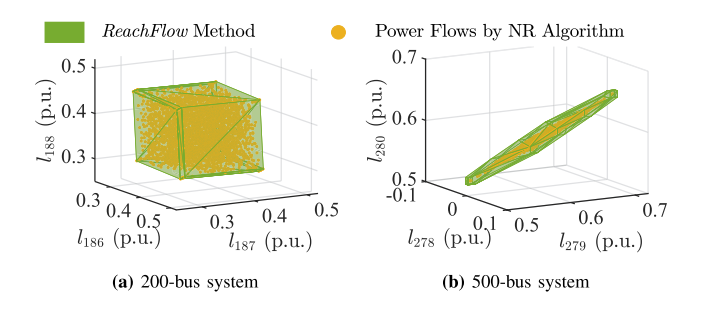


Fig. 5. Macrogrid ReachFlow results ( $l_i$ : active power flow of the  $i_{th}$  branch.).

the microgrid ReachFlow, where the green area is a projection of the high-dimensional ReachFlow zonotope and the yellow dots represents the massive NR power flow results obtained by sampling  $\mathcal{U}^0$  exhaustively. The zonotope rigorously encloses all the power flow results, which verifies ReachFlow's correctness and tight overapproximation feature.

2) Macrogrid ReachFlow: Fig. 5 shows the ReachFlow results of two macrogrids which are modified from MATPOWER's repository [26] by adding primary frequency controls and incorporating frequency-dependent impedance loads and lines. The RE penetration is set up as 10% with 20% uncertainty.

Static power flow results are found entirely and tightly contained by the *ReachFlow* results, which verifies the applicability of *ReachFlow* to macrogrids. Interestingly, Fig. 5(a) show weak correlations of the power flows through three branches whereas Fig. 5(b) shows rather strong couplings. This is because the former branches are connected directly to three RE generators with independent uncertainties while the latter are tied to three

TABLE I COMPUTING TIME OF *REACHFLOW* 

Test system	ReachFlow	Monte Carlo (3,000 runs)
33-bus microgrid	27.18s	22.46s
200-bus macrogrid	89.32s	124.89s
500-bus macrogrid	430.66s	749.46s

TABLE II
ACCURACY COMPARISON BETWEEN REACHFLOW AND MONTE CARLO

Test system	ReachFlow	Monte Carlo (3,000 runs)
33-bus microgrid	103.60%	87.75%
200-bus macrogrid	107.72%	86.12%
500-bus macrogrid	108.96%	90.27%

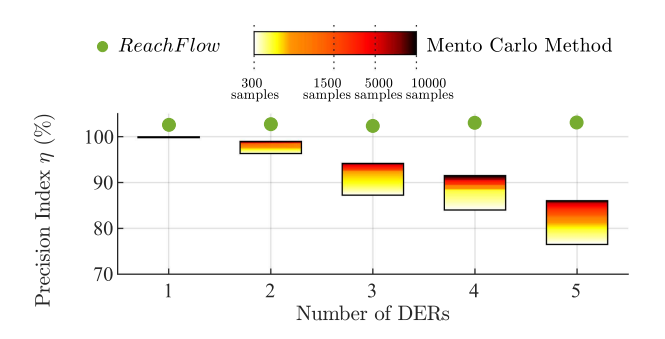


Fig. 6. ReachFlow vs. Monte Carlo (the precision index for Monte Carlo is also applied to ReachFlow).

dispatchable power plants. Hence the power flow fluctuations in the latter case are significantly less impacted by the RE uncertainties. Table I gives the computational costs for a microgrid with complicated DER controllers and two macrogrids. *ReachFlow* exhibits excellent computational efficiency and is more efficient than a very light Monte Carlo of 3,000 runs.

3) ReachFlow Vs. Existing Methods (Monte Carlo, Intervaland Ellipsoid- Based Methods): ReachFlow is compared with Monte Carlo by using the 33-bus microgrid. An index  $\eta$  is adopted to quantify the precision of Monte Carlo results:

$$\eta = \operatorname{mean}\left(\frac{\max_{j}(\boldsymbol{x}_{j}^{MC}) - \min_{j}(\boldsymbol{x}_{j}^{MC})}{\sup \boldsymbol{x} - \inf \boldsymbol{x}}\right)$$
(29)

where  $x_i^{MC}$  denotes the power flow solution of the j-th Monte Carlo trial;  $\sup x$  and  $\inf x$  denote the supremum and infimum of x obtained by traversing the uncertainty space  $\mathcal{U}^0$ . Upon this definition,  $\eta > 1$  means a conservative estimation of the power flow bounds while  $\eta < 1$  an under estimation. A tight estimation can be achieved when  $\eta$  is close to 1. Table II presents the quantitative comparison between ReachFlow and Monte Carlo based on the precision index  $\eta$ . ReachFlow successfully achieves conservative but tight estimation of the power flow states (i.e.,  $\eta$  is larger than but very close to 1). Whereas, Monte Carlo induces underestimated results, which indicates that some extreme power flow conditions are missed. Using such overly optimistic assessments in system operations or planning would likely lead to catastrophe hazards in the utility grids. Further, Fig. 6 takes the 33-bus microgrid to investigate the impact of the uncertainty dimension. Simulation results indicate that with

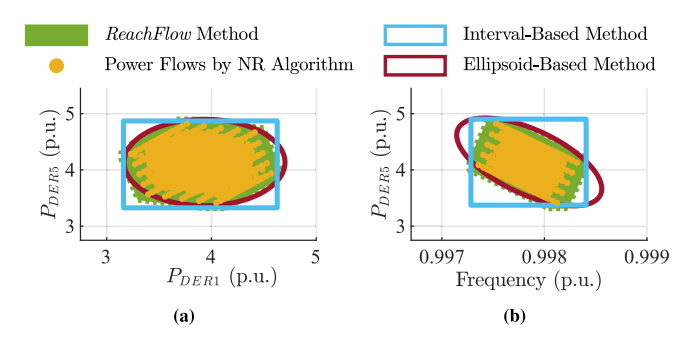


Fig. 7. ReachFlow vs. existing set-based methods.

Test system	ReachFlow	Ellipsoid-based method	Interval-based method
33-bus microgrid	114.30%	139.49%	148.41%
200-bus macrogrid	122.90%	149.59%	161.95%
500-bus macrogrid	121.32%	146.46%	179.45%

an increased number of uncertain factors (i.e., the number of DERs), the precision of Monte Carlo results declines sharply. Even worse, increasing the sample size fails to improve the precision. *ReachFlow*, conversely, always provides rigorous estimations with restricted conservativeness as shown in Fig. 6. In summary, *ReachFlow* outperforms Monte Carlo simulation from two aspects: i) it is capable of obtaining the set of power flow results in a single run, whereas Monte Carlo requires running power flow repeatedly under different uncertain scenarios; ii) it is efficacious in handling the high-dimensional uncertainties, whereas Monte Carlo suffers from the curse of dimensionality when sampling the entire uncertainty space.

ReachFlow is further compared with two other set presentations, i.e., multi-dimensional intervals [12] and ellipsoids [14]. As shown in Fig. 7, both interval and ellipsoid power flow solutions suffers from overly conservative estimations due to the dependencies among power system variables. The ellipsoid method performs better than interval analysis method for certain scenarios, as shown in Fig. 7(a), where the ellipsoid calculated is rather tight. For other scenarios, e.g. when the selected power flow states are coupled, the ellipsoid results can be excessively conservative, as shown in Fig. 7(b). In contrast, our zonotope-based ReachFlow always provides tight over-approximations, making it a much more dependable tool as compared to interval or ellipsoid methods.

Table III further presents the quantitative comparison. An index  $\xi$  is adopted to quantify the precision of *ReachFlow* and the set-based methods:

$$\xi = \operatorname{mean}_{i,j} \frac{\sqrt{\operatorname{Area}(\operatorname{proj}(\mathcal{S}, i, j))}}{\sqrt{\operatorname{Area}(\operatorname{proj}(\mathcal{S}_{PF}, i, j))}}$$
(30)

where  $Area(\cdot)$  denotes the area computation function;  $proj(\mathcal{S}, i, j)$  projects the set  $\mathcal{S}$  to the i-j plane;  $\mathcal{S}$  denotes the power flow set described by zonotope (i.e., by ReachFlow), ellipsoid or multi-dimensional intervals;  $\mathcal{S}_{PF}$  denotes the real region of uncertain power flow states, which is estimated by

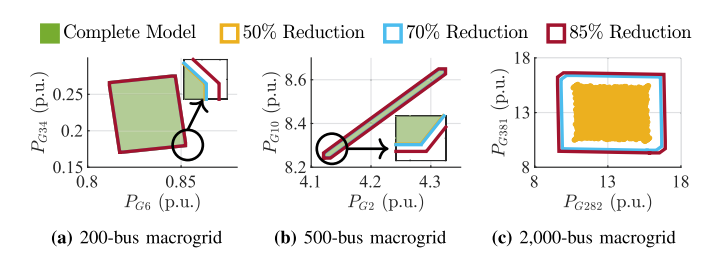


Fig. 8.  $ReachFlow^R$  results with different reduction ratios ( $P_{Gi}$ : active power output of the  $i_{th}$  generator).

 $\begin{array}{c} {\rm TABLE\ IV} \\ {\rm Computing\ Time\ of}\ ReachFlow^R \end{array}$ 

Test	reduction ratio			
system [26]	0 (complete model)	50%	70%	85%
200-bus	89.32s	30.65s	17.98s	14.59s
500-bus	430.66s	132.44s	75.95s	48.35s
2,000-bus	\ 1	> 1 hour	1876.90s	846.19s

<sup>1</sup>PC runs out of memory.

traversing the uncertainty space.  $\xi$  reflects the averaged area of each 2-dimensional projection of the power flow set. Obviously, if  $\mathcal{S}$  encloses  $\mathcal{S}_{PF}$ , each projection of  $\mathcal{S}$  encloses the projection of  $\mathcal{S}_{PF}$ . Further, a perfect estimation of  $\mathcal{S}_{PF}$  ensures that each projection of  $\mathcal{S}$  matches the projection of  $\mathcal{S}_{PF}$ . Therefore, a tighter estimation is achieved when  $\xi$  is closer to 1. Results in Table III show that among all these methods, the zonotope-based ReachFlow provides the tightest estimation, which is coincident with the observations in Fig. 7. This again verifies the accuracy and flexibility of ReachFlow in quantifying the uncertain power flow states.

# B. Validity of $ReachFlow^R$ and $ReachFlow^P$

ReachFlow calculation is of high computational complexity as indicated by Table I. This Subsection verifies two practical ReachFlow variants,  $ReachFlow^R$  and  $ReachFlow^P$ , to demonstrate their applicability for large-scale power systems.

1) Reduced-Order ReachFlow: For the 200-bus, 500-bus and 2,000-bus macrogrids, the  $ReachFlow^R$  results always enclose the ReachFlow results or the Monte Carlo results, offering guaranteed over-approximations. Note that higher reduction ratio leads to larger over-approximation (see Fig. 8). As a rule of thumb, a 70% reduction ratio or so can give satisfactory  $ReachFlow^R$  results with restricted conservativeness.

Table IV shows that  $ReachFlow^R$ 's computational efficiency improves with increased reduction ratio. A daunting fact is that ReachFlow can no longer solve reachable power flow for the 2,000-bus power system on a PC, while  $ReachFlow^R$  successfully produces an satisfactory enclosure of the reduced-order power flows within acceptable computing time.

2) Parallel ReachFlow: The correctness of ReachFlow<sup>P</sup> is verified as it ensures an enclosure of the ReachFlow results, as shown in Fig. 9.  $ReachFlow^P$  on more cores yields higher efficiency (see Table. V) at a cost of reduced tightness. This is understandable because the parallelized sub-ReachFlow s,

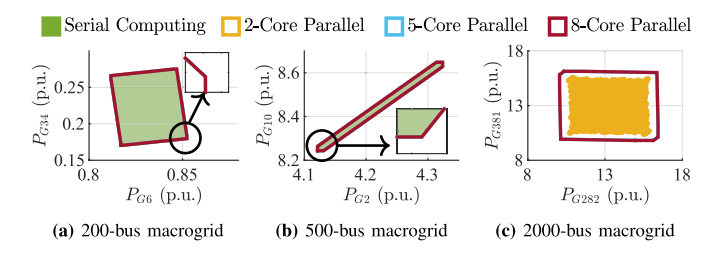


Fig. 9. ReachFlow P results with different number of cores.

TABLE V COMPUTING TIME OF  $ReachFlow^F$ 

Test	Number of Cores			
system	1 (serial computing)	2	5	8
200-bus	89.32s	33.56s	21.62s	16.14s
500-bus	430.66s	180.86s	70.93s	40.89s
2,000-bus	\ 1	> 1 hour	1495.34s	829.78s

<sup>&</sup>lt;sup>1</sup>PC runs out of memory

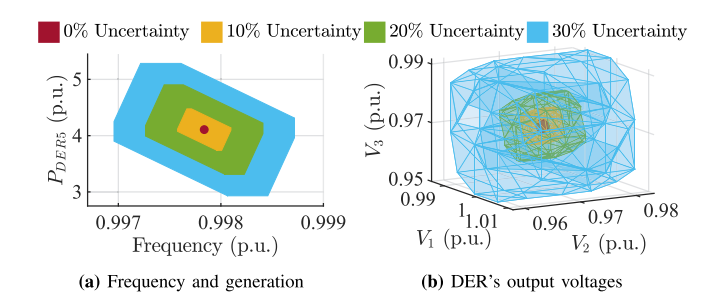


Fig. 10. Impact of the uncertainty level on ReachFlow.

as presented in (23), cannot fully incorporate their inherent couplings, which leads to over-approximation.

Compared with Fig. 8, it is observed that  $ReachFlow^P$  is tighter than  $ReachFlow^R$ . The reason is that  $ReachFlow^P$  formulates the range of each subset of power flow states by a zonotope, and hence reduces the over-approximation compared with  $ReachFlow^R$  which formulates the eliminated power flow states roughly by intervals. Both  $ReachFlow^R$  and  $ReachFlow^P$  enhance the scalability of ReachFlow for large-scale power systems. Compared with  $ReachFlow^R$ ,  $ReachFlow^P$  is capable of obtaining the overall ReachFlow via each sub-ReachFlow, while  $ReachFlow^R$  only outputs the reachable set of the selected power flow states.

# C. ReachFlow-Based Power Flow Control Strategy Analysis

ReachFlow serves as a formal tool to verify the efficacy of power flow control strategies against uncertainties. This Subsection exemplifies the use of ReachFlow to analyze the impact of renewable energy (RE) integration and verify droop and secondary control in the 33-bus microgrid. By default, the microgrid is fully supported by the renewable energy with 20% uncertainty.

1) Impact of Renewable Energy (RE) Integration: Fig. 10 investigates ReachFlow under different uncertainty levels with

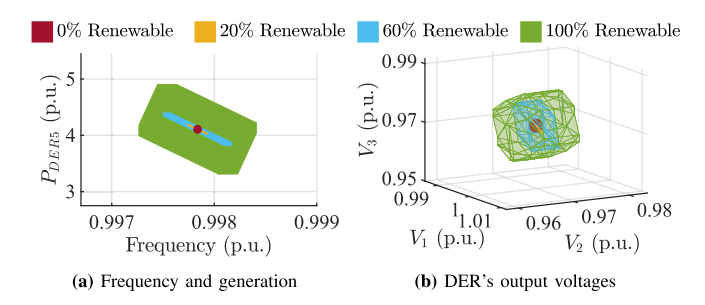


Fig. 11. Impact of the renewable energy penetration on ReachFlow.

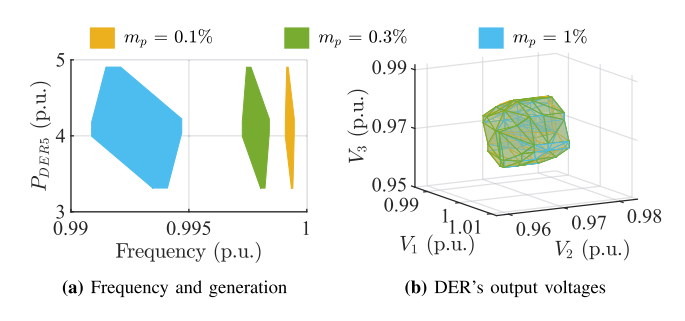


Fig. 12. Impact of active power droop coefficient  $m_p$  on ReachFlow.

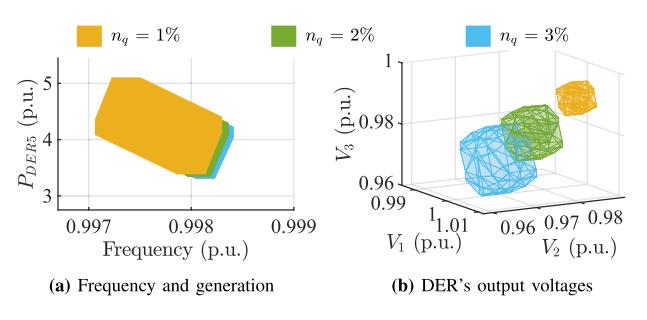


Fig. 13. Impact of reactive power droop coefficient  $n_q$  on ReachFlow.

droop control only. With the increase of uncertainties, *Reach-Flow* expands accordingly, indicating large deviations of the power flow states driven by DER fluctuations.

Fig. 11 further studies the impact of RE penetration. The growing penetration of RE leads to expanded *ReachFlow* because of both the increased uncertainties from the DERs and the decreased regulating ability of the fully controllable generators. Specifically, in the scenario with no RE sources, *ReachFlow* degenerates to a single point (see the red dot), which indicates that the uncertain power flow degenerates to the static power flow with only conventional generators.

2) Performance of Droop Control: Fig. 12 and Fig. 13 respectively study the ReachFlow with different droop gains  $m_p$  or  $n_q$ . The droop control logic is presented in (2a) and (3a). Simulation indicates that  $m_p$  strongly impacts the zonotope of system frequency and that  $n_q$  is closely correlated to the zonotope of bus voltages, which follows the droop control logic. In addition, it can be observed that the system frequency/voltages can not be maintained at their nominal values, which indicates that droop control results in steady-state deviations.

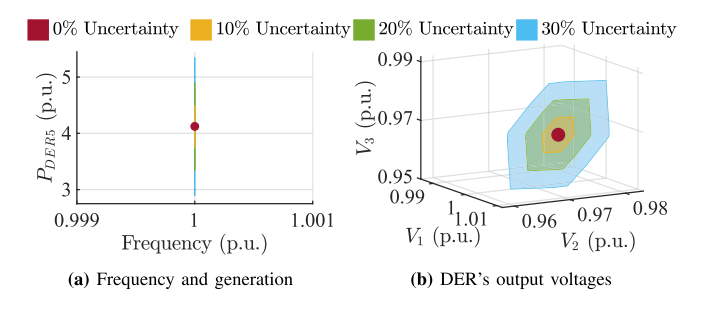


Fig. 14. Efficacy of secondary control verified via ReachFlow.

By examining different levels of uncertainties, one can find that the increase in  $m_p$  or  $n_q$  leads to expanded *ReachFlow*, meaning increased droop gains exacerbate uncertainties in power flow states and thus drastically affect microgrid security.

3) Performance of Secondary Control: Fig. 14 shows a surprise finding that, with secondary control, the reachable set of P-f (i.e., active power generation of DER vs. microgrid frequency) degenerates to a line, while the reachable set of  $V_1-V_2-V_3$  (i.e., output-voltage magnitudes of DERs) degenerates to a plane. This reflects that the secondary control successfully maintain the system frequency and the output voltage of DER1 at 1 p.u., despite any uncertainty level. By comparing Fig. 14 with Fig. 10, it can be seen that the secondary control realizes disturbance rejections and error-free as long as there exist sufficient reserves in DERs.

*ReachFlow* and its variants therefore offers powerful tools to formally verify power flow control strategies under structural and parametric uncertainties.

#### VII. CONCLUSION

This paper offers three innovations imperative to make ReachFlow practical: formal proofs of ODE-PF stability, a  $ReachFlow^R$  and a  $ReachFlow^P$  that jointly scale up ReachFlow for ultra-scale power flow problems. The stable ODE-PF model enables ReachFlow to be a non-divergent power flow solver.  $ReachFlow^R$  generates the reachable set of selected power flow states and is flexible enough to be implemented on any computers.  $ReachFlow^P$  decomposes the time-consuming reachability analysis into parallel-enabled lower-dimensional reachable set calculations well-suited for implementation on multi-core computers or computer clusters. Next, a privacy-reserving and more accurate ReachFlow is to be developed.

# APPENDIX ALGORITHM FOR REACHABLE SET EVOLUTION

#### A. Over-Approximation of Linear Abstraction in ReachFlow

The time-point solution of linear dynamics can be separated into the homogeneous part  $z^h$  and the inhomogeneous part  $z^p$ :

$$\begin{cases}
\boldsymbol{z}^{h}((k+1)\tau) = e^{\boldsymbol{A}\tau}\boldsymbol{z}^{h}(k\tau) \\
\boldsymbol{z}^{p}((k+1)\tau) = e^{\boldsymbol{A}\tau}\boldsymbol{z}^{p}(k\tau) + \boldsymbol{A}^{-1}(e^{\boldsymbol{A}\tau} - \boldsymbol{I})f(\boldsymbol{z}^{*})
\end{cases} (31)$$

Hence, the reachable set for the linear abstraction of (16) at time point  $(k+1)\tau$  is computed based on the reachable set at the previous time-point  $\mathcal{R}(k\tau)$  [27]:

$$\mathcal{R}^{lin}((k+1)\tau) = \{\boldsymbol{z}^h(t) + \boldsymbol{z}^p(t) | t = (k+1)\tau\}$$

$$= e^{\boldsymbol{A}\tau}(\mathcal{R}(k\tau) - \boldsymbol{z}^*) \oplus \boldsymbol{A}^{-1}(e^{\boldsymbol{A}\tau} - \boldsymbol{I})\boldsymbol{f}(\boldsymbol{z}^*) \oplus \boldsymbol{z}^*$$
(32)

Further, the time-interval reachable set during  $[k\tau, (k+1)\tau]$  can be enclosed by [27]:

$$\mathcal{R}_{k}^{lin} = \{ \boldsymbol{z}(k\tau + \Delta t) | \Delta t \in [0, \tau] \} 
\subseteq \{ \boldsymbol{z}(k\tau) + \frac{\Delta t}{\tau} (\boldsymbol{z}((k+1)\tau) - \boldsymbol{z}(k\tau)) + \mathcal{F}\boldsymbol{z}(k\tau) \} 
\subseteq \mathbf{conv}(\mathcal{R}(k\tau), \mathcal{R}^{lin}((k+1)\tau)) \oplus \mathcal{F}(\mathcal{R}(k\tau) - \boldsymbol{z}^{*}) 
\triangleq \text{LinearReach}(\mathcal{R}(k\tau), \boldsymbol{z}^{*}, \boldsymbol{f}(\boldsymbol{z}^{*}), \boldsymbol{A}, \tau)$$
(33)

where **conv** denotes the convex hull of two sets;  $\mathcal{F} = \sum_{i=2}^{\eta} [(i^{\frac{-i}{i-1}} - i^{\frac{-1}{i-1}})\tau^i, 0] \frac{A^i}{i!} \oplus \mathcal{E}(\tau)$  is an interval matrix to ensure the necessary conservativeness [27].

## B. Over-Approximation of Linearization Error in ReachFlow

Given the maximum value of  $\mathcal{L}$ , i.e.,  $\overline{\mathcal{L}}$ , the set of linearization error can be over-approximated as [22]:

$$\mathcal{R}_{k}^{err} = \mathcal{F}_{2}[-\overline{\mathcal{L}}, \overline{\mathcal{L}}] \triangleq \text{ErrorReach}(\overline{\mathcal{L}}, \boldsymbol{A}, \tau)$$
 (34)

where  $\mathcal{F}_2 = \sum_{i=0}^{\eta} \frac{A^i \tau^{i+1}}{(i+1)!} \oplus \mathcal{E}(\tau) \tau$  encloses  $A^{-1}(e^{A\tau} - I)$  in analogy with the inhomogeneous solution in (31).

#### REFERENCES

- [1] International Energy Agency, "World energy outlook 2019," 2019. [Online]. Available: http://www.nea.gov.cn/2019-01/28/c\_137780779.htm
- [2] W. Zappa, M. Junginger, and M. van den Broek, "Is a 100% renewable European power system feasible by 2050?," Appl. energy, vol. 233, pp. 1027–1050, 2010.
- [3] M. M. Hand et al., "Renewable electricity futures study. Volume 1. Exploration of high-penetration renewable electricity futures," National Renewable Energy Lab. (NREL), Golden, CO, USA, Tech. Rep. NREL/TP-6A20-52409-1, 2012.
- [4] P. Zou, Q. Chen, Y. Yu, Q. Xia, and C. Kang, "Electricity markets evolution with the changing generation mix: An empirical analysis based on China 2050 high renewable energy penetration roadmap," *Appl. energy*, vol. 185, pp. 56–67, 2017.
- [5] R. Y. Rubinstein and D. P. Kroese, Simulation and the Monte Carlo Method. Hoboken, NJ, USA: Wiley, 2016.
- [6] E. Zio, M. Delfanti, L. Giorgi, V. Olivieri, and G. Sansavini, "Monte Carlo simulation-based probabilistic assessment of DG penetration in medium voltage distribution networks," *Int. J. Elect. Power Energy Syst.*, vol. 64, pp. 852–860, 2015.
- [7] X. Xu and Z. Yan, "Probabilistic load flow calculation with Quasi-Monte carlo and multiple linear regression," *Int. J. Elect. Power Energy Syst.*, vol. 88, pp. 1–12, 2017.
- [8] M. Kabir, Y. Mishra, and R. Bansal, "Probabilistic load flow for distribution systems with uncertain PV generation," *Appl. Energy*, vol. 163, pp. 343–351, 2016.
- [9] M. Aien, A. Hajebrahimi, and M. Fotuhi-Firuzabad, "A comprehensive review on uncertainty modeling techniques in power system studies," *Renewable Sustain. Energy Rev.*, vol. 57, pp. 1077–1089, 2016.
- [10] Z. Ren, W. Li, R. Billinton, and W. Yan, "Probabilistic power flow analysis based on the stochastic response surface method," *IEEE Trans. Power Syst.*, vol. 31, no. 3, pp. 2307–2315, May 2016.
- [11] M. Fan, V. Vittal, G. T. Heydt, and R. Ayyanar, "Probabilistic power flow analysis with generation dispatch including photovoltaic resources," *IEEE Trans. Power Syst.*, vol. 28, no. 2, pp. 1797–1805, 2012.

- [12] Z. Wang and F. L. Alvarado, "Interval arithmetic in power flow analysis," IEEE Trans. Power Syst., vol. 7, no. 3, pp. 1341–1349, Aug. 1992.
- [13] C. Zhang, H. Chen, K. Shi, M. Qiu, D. Hua, and H. Ngan, "An interval power flow analysis through optimizing-scenarios method," *IEEE Trans. Smart Grid*, vol. 9, no. 5, pp. 5217–5226, Sep. 2018.
- [14] X. Jiang, Y. C. Chen, and A. D. Domínguez-García, "A set-theoretic framework to assess the impact of variable generation on the power flow," *IEEE Trans. Power Syst.*, vol. 28, no. 2, pp. 855–867, May 2013.
- [15] A. T. Saric and A. M. Stankovic, "Applications of ellipsoidal approximations to polyhedral sets in power system optimization," *IEEE Trans. Power Syst.*, vol. 23, no. 3, pp. 956–965, 2008.
- [16] X. Jiang and A. D. Domínguez-García, "A zonotope-based method for capturing the effect of variable generation on the power flow," in *Proc. IEEE North Amer. Power Symp.*, 2014, pp. 1–6.
- [17] J. Gao, B. Han, C. Xu, L. Zhang, G. Li, and K. Wang, "Zonotope-based quantification of the impact of renewable power generation on hybrid ac/dc distribution system," *J. Eng.*, vol. 2019, no. 16, pp. 2493–2499, 2019.
- [18] Y. Zhou and P. Zhang, "Reachable power flow," *IEEE Trans. Power Syst.*, vol. 35, no. 4, pp. 3290–3293, Jul. 2020.
- [19] N. Kochdumper and M. Althoff, "Reachability analysis for hybrid systems with nonlinear guard sets," in *Proc. 23rd Int. Conf. Hybrid Syst.: Comput. Control*, 2020, pp. 1–10.
- [20] F. Feng and P. Zhang, "Enhanced microgrid power flow incorporating hierarchical control," *IEEE Trans. Power Syst.*, vol. 35, no. 3, pp. 2463–2466, May 2020.
- [21] N. Pogaku, M. Prodanovic, and T. C. Green, "Modeling, analysis and testing of autonomous operation of an inverter-based microgrid," *IEEE Trans. Power Electron.*, vol. 22, no. 2, pp. 613–625, Mar. 2007.
- [22] B. Schürmann, N. Kochdumper, and M. Althoff, "Reachset model predictive control for disturbed nonlinear systems," in *Proc. IEEE Conf. Decis. Control*, 2018, pp. 3463–3470.
- [23] G. M. Ziegler, Lectures on Polytopes. Berlin, Germany: Springer, 2012, vol. 152.
- [24] M. Althoff and N. Kochdumper, "Cora toolbox," 2018. [Online]. Available: https://tumcps.github.io/CORA/
- [25] G. Díaz, J. Gómez-Aleixandre, and J. Coto, "Direct backward/forward sweep algorithm for solving load power flows in AC droop-regulated microgrids," *IEEE Trans. Smart Grid*, vol. 7, no. 5, pp. 2208–2217, Sep. 2016.
- [26] R. D. Zimmerman, C. E. Murillo-Sánchez, and R. J. Thomas, "Matpower: Steady-state operations, planning, and analysis tools for power systems research and education," *IEEE Trans. Power Syst.*, vol. 26, no. 1, pp. 12–19, Feb. 2011.

[27] M. Althoff, "Reachability analysis of large linear systems with uncertain inputs in the Krylov subspace," *IEEE Trans. Autom. Control*, vol. 65, no. 2, pp. 477–492, Feb. 2020.



Yifan Zhou (Member, IEEE) received the B.S. and Ph.D. degrees from Tsinghua University, Beijing, China, in 2014 and 2019, respectively, both in electrical engineering. She is currently a Postdoctoral Researcher with Stony Brook University, Stony Brook, NY, USA. Her research interests include microgrid stability and control, formal methods and reachability analysis, and quantum computing.



Peng Zhang (Senior Member, IEEE) received the Ph.D. degree in electrical engineering from the University of British Columbia, Vancouver, BC, Canada, in 2009. He is a SUNY Empire Innovation Professor with Stony Brook University, New York, NY, USA. He has a joint appointment at Brookhaven National Laboratory as a Staff Scientist. Previously, he was a Centennial Associate Professor and a Francis L. Castleman Associate Professor with the University of Connecticut, Storrs, CT, USA. He was a System Planning Engineer with BC Hydro and Power Authority,

Canada, from 2006 to 2010. His research interests include programmable microgrids, networked microgrids, quantum security, quantum computing, power system stability and control, cyber security, formal methods and reachability analysis, and software-defined networking.

Dr. Zhang is an Individual Member of CIGR É. He is an Editor for the IEEE TRANSACTIONS ON POWER SYSTEMS, the IEEE TRANSACTIONS ON SUSTAINABLE ENERGY and the IEEE POWER AND ENERGY SOCIETY LETTERS, and an Associate Editor for the IEEE JOURNAL OF OCEANIC ENGINEERING.